Supplementary Data

Effects of Post-Transcriptional Regulation on Phenotypic Noise in *E. coli*

Rinat Arbel-Goren[1], Asaf Tal[1], Tamar Friedlander[2], Shiri Meshner[1], Nina Costantino[3], Donald L. Court[3] and Joel Stavans[1,*]

[1]Department of Physics of Complex Systems

[2]Department of Molecular Cell Biology

Weizmann Institute of Science

Rehovot 76100, Israel

[3]Gene Regulation and Chromosome Biology Laboratory

Frederick National Laboratory for Cancer Research,

National Cancer Institute

Frederick, MD, USA

[*] joel.stavans@weizmann.ac.il

Contents

Supplementary Tables

Supplementary Figures

Supplementary Methods

11. Stochastic simulations of two genes whose expression is controlled by a sRNA

Supplementary Text

1. Intrinsic noise dominates phenotypic variability for small values of the mean protein concentration μ_p
2. Extrinsic noise sources can produce a linear dependence of σ_p on μ_p
3. Attempts to measure intrinsic noise in SodB synthesis using strains bearing dual chromosomal *sodB* genes

Supplementary References

Supplementary Tables

Table S1 Parameter values used in the simulations**.**

parameter	symbol	value [1/min]	Reference
sRNA-mRNA binding rate	$k_{4,5}$	0.02	(1)
translation rates	$k_{6,7}$	1	(1)
mRNA decay	$k_{8,9}$	0.04	(1)
sRNA decay	k_{10}	0.0231	
protein dilution through cell division	$k_{11,12}$		30 minutes cell cycle
inactive to active transition rate (bursting)	k_{on}	0.42	(2)
active to inactive transition rate of mRNA1 production (bursting)	k_{off1}	5.376	(2)
active to inactive transition rate of mRNA2 production (bursting)	k_{off2}	11.17	(2)
active to inactive transition rate of sRNA production (bursting)	$k_{\mathrm{off\_s}}$	$k_{\mathrm{on}} * (k_{\mathrm{tx}} - k_3)/k_3$	(2)
transcription rate (bursting)	k_{tx}	13.8	(2)

Parameters in the last four lines were used only if bursting in transcription was implemented.

Table S2 Sequences of primers used for clone and plasmid preparation

Primer	**Sequence (5' to 3')**
sodB PCR1 up	AAACGAAAGGCTCAGTGCAAAGCTTGGGCCTTTCGTTTTATCTGTTG TTTAATTAACCCTCACTAAAGGGCG
sodB PCR1 down	CCTAGGTCTAGGGCGGCGGATTTGTCCTACTCAGGAGAGCGTTCACC GACTAATACGACTCACTATAGGGC
sodB PCR2 up	ACTTCTGGGCGCTGGTGAACTGGGAATTCGTAGCGAAAAATCTCGCT GCCAGGATCCGCTGGCTCCGCTGCTGGTTCTGGCGAATTCATGCGTA AAGGAGAAGAACTTTTC
sodB PCR2 down	CCTGATAAGCGTAGCGCTTCAGGCAATGCTGCATTTGCCATCAGTTA TTATAATACGACTCACTATAGGGC
cfp up	ACTTGTCACTACTTTGACTTGGGG
cfp down	GGTCTGCTAGTTGAACGCTTCC
fumA PCR up	AGCACGTGTTGACAATTAATCATCG
fumA PCR down	ACCATTTGATAACAAATGTTTGGTCTTTCGTGCCATGTAAAAAAACCG CCCGAAGGGCGGCTCTGTTTATAATACGACTCACTATAGGGC
fumA PCR c up	GGCTTCTACCTTGGCAGTATCGG
fumA PCR c down	CGCATGAATCAGTGAGGTGGG
sodB PCR3 up	ACCGGTTCTCAGTGAAGACTACTGG
sodB PCR3 down	GAATTCTGCTACTCTCCTTTATTATTAATTTG
fumA PCR4 up	ACCGGTCTGGACGGATTTTCCATAC
fumA PCR4 down	GAATTCTGTTCTCTCACTTACTGC
yfp c up	CATGCCCGAAGGTTATGTACAGG
yfp c down	GGGCAGATTGATAGGACAGGTAATGG
ryhB up	TTTGCAAAAAGTGTTGGACAAGTGCGAATGAGAATGATTATTATTGT CTCTCCTAATTTTTGTTGACACTCTA

Primer	**Sequence (5' to 3')**
ryhB down	TAACGAACAAAGCACTCCCGTGGATAAATTGAGAACGAAAGATCAAA AACTCTTGGGTTATCAAGAGGG

Table S3 Mean protein copy-number of selected sRNAs targets in *E. coli*

sRNA	Gene Name	Description	MeanProtein	Reference
RhyB	**fumA**	Fumarate hydratase class I, aerobic (EC 4.2.1.2) (Fumarase)	315, 130	(3), this article
	sodB	Superoxide dismutase, Fe; response to oxidative stress	350	this article
	fur	DNA-binding transcriptional dual regulator of siderophore biosynthesis and transport	193.2	(4)
	sdhCDAB	2-oxoglutarate dehydrogenase E1 component (EC 1.2.4.2) (Alpha-ketoglutarate dehydrogenase)	1330	(3)
	iscS	Cysteine desulfurase (EC 2.8.1.7) (ThiI transpersulfidase) (NifS protein homolog)	3650	(3)
	sucD	Succinyl-CoA synthetase alpha chain (EC 6.2.1.5) (SCS-alpha)	2420	(3)
	rne	Ribonuclease E (EC 3.1.4.-) (RNase E)	477	(3)
	sdhD	D-serine dehydratase (EC 4.3.1.18) (D-serine deaminase) (DSD)	147	(3)
	ftnA	Ferritin 1	1910	(3)
	ACO1	Aconitate hydratase 1 (EC 4.2.1.3) (Citrate hydro-lyase 1) (Aconitase 1)	198	(3)
	bfrL	Bacterioferritin (BFR) (Cytochrome B-1) (Cytochrome B-557)	289	(3)
Spot42	**glpFK**	Glycerol kinase (EC 2.7.1.30) (ATP:glycerol 3-phosphotransferase) (Glycerokinase) (GK)	1160	(3)
	gltA	citrate synthase	1390 and 89.1	(3) , (4)
FnrS	**gpmA**	phosphoglyceromutase 1	760.1	(4)
	cydD	fused cysteine transporter subunits of ABC superfamily: membrane component -!- ATP-binding component	15.8	(4)
CyaR	**nadE**	NAD synthetase; NH3/glutamine-dependent	30.9	(4)
SgrS	**manX**	fused mannose-specific PTS enzymes: IIA component -!- IIB component	57.9	(4)
Oxys	**cspC**	stress protein; member of the CspA-family	7890.5	(4)
	dps	Fe-binding and storage protein	8.7 and 3730	(3), (4)
	wrbA	predicted flavoprotein in Trp regulation	219.1	(4)

sRNA	Gene Name	Description	MeanProtein	Reference
Oxys	**pqqL**	predicted peptidase	0.9	(4)
	hdeA	stress response protein acid-resistance protein	21.1	(4)
	oxyR	DNA-binding transcriptional dual regulator	79.1	(4)
	wrbA	predicted flavoprotein in Trp regulation	220, 1220	(3), (4)
GcvB	**gltI**	glutamate and aspartate transporter subunit -!- periplasmic-binding component of ABC superfamily	0.2	(4)
	argT	lysine/arginine/ornithine transporter subunit -!- periplasmic-binding component of ABC superfamily	1.6	(4)
	ndk	multifunctional nucleoside diphosphate kinase and apyrimidinic endonuclease and 3'-phosphodiesterase	178.2	(4)
	iciA	DNA-binding transcriptional activator; replication initiation inhibitor	33.4	(4)
	livJ	leucine/isoleucine/valine transporter subunit -!- periplasmic-binding component of ABC superfamily	8.1, 4	(3), (4)
	livk	Leucine-specific binding protein precursor (LS-BP) (L-BP)	424	(3)
	oppA	Periplasmic oligopeptide-binding protein precursor	12000	(3)
	agrT	Lysine-arginine-ornithine-binding periplasmic protein precursor (LAO-binding protein)	212	(3)
	dppA	Periplasmic dipeptide transport protein precursor (Dipeptide-binding protein) (DBP)	565	(3)
Ssra	**prsA**	phosphoribosylpyrophosphate synthase	283.2	(4)
	relE	Qin prophage; toxin of the RelE-RelB toxin-antitoxin system	1.9	(4)
	smpB	trans-translation protein	14.7	(4)
	sspB	ClpXP protease specificity-enhancing factor	45.5	(4)
	tufa	protein chain elongation factor EF-Tu	3350.2	(4)
	fusA	protein chain elongation factor EF-G	316.4	(4)
	rspA	predicted dehydratase	0.2	(4)
	tufB	protein chain elongation factor EF-Tu (duplicate of tufA)	2202.8	(4)

sRNA	Gene Name	Description	Mean_Protein	Reference
RybB	**ompA**	Outer membrane protein A precursor (Outer membrane protein II*)	29900	(3)
	ompC	outer membrane porin protein C	0.8 , 3560	(4), (3)
	rbsB	D-ribose transporter subunit -!- periplasmic-binding compoent of ABC superfamily	0.2	(4)
	flu	CP4-44 prophage; antigen 43 (Ag43) phase-variable biofilm formation autotransporter	2.3	(4)
	fumC	fumarate hydratase (fumarase C); aerobic Class II	20.8	(4)
	tsx	Nucleoside-specific channel-forming protein tsx precursor	2830	(3)
	rluD	Ribosomal large subunit pseudouridine synthase D (EC 4.2.1.70) (Pseudouridylate synthase)	176	(3)
	fadL	Long-chain fatty acid transport protein precursor (Outer membrane fadL protein)	420	(3)
OmrA,B	**ompR**	DNA-binding response regulator in two-component regulatory system with EnvZ	80.8, 613	(3), (4)
	csgD	DNA-binding transcriptional activator in two-component regulatory system	23.3	(4)
	ompF	Outer membrane protein F precursor (Porin ompF) (Outer membrane protein 1A) (Outer membran	1250	(3)
	fliY	Cystine-binding periplasmic protein precursor (CBP) (fliY protein) (Sulfate starvation-ind	955	(3)
	cirA	Colicin I receptor precursor	483	(3)
	ompT	Protease VII precursor (EC 3.4.21.87) (Omptin) (Outer membrane protein 3B) (Protease A)	2590	(3)
	ompX	Outer membrane protein X precursor	31200	(3)
	fecA	Iron(III) dicitrate transport protein fecA precursor	358	(3)
	sdhM	L-serine dehydratase 2 (EC 4.3.1.17) (L-serine deaminase 2) (SDH 2) (L-SD2)	488	(3)
	btuB	Vitamin B12 receptor precursor	238	(3)
	sdhC	Serine transporter	664	(3)
OmrA,B	**yejF**	Hypothetical ABC transporter ATP-binding protein yejF	106	(3)

sRNA	Gene Name	Description	Mean_Protein	Reference
OmrA,B	**yohN**	Hypothetical protein yohN precursor	453	(3)
	acsA	Acetyl-coenzyme A synthetase (EC 6.2.1.1) (Acetate--CoA ligase) (Acyl-activating enzyme)	112	(3)

Table S4 Sequences of smFISH probes

Transcript	Probe sequences (5'to 3')
FumA	gctggttagcaggtaatact attcagatacgctaacgtgt gcgactttcaaaatctcctg caacagagttaacgcttcgg atgaacgacgcatcatgaaa tttatcattttcgctggcct gagttacgcaggaattgcag gtatcctgacaggttggcag taccaacaataatcgcggtg taagtgttatagacaccgcg agtagcgcagattatcttcg tttatacatatccagcggcg cagattggtgccggtattca cataaagatcgatctgcgct tttgtattcgtcgccatcaa ccacctttggcgatacagag gatacgtcttgtttgccgaa aacgctttggtttcctgata gcatcttctcaaccaggtaa atatgatacggaggacaggc agttccaccaataacgaacg ccgttttaaggttcgtttct tatttcgcggaagccagttt ttccgttggcagttcatcat ttttccagttccacatcgcg aagattttgcgcttcgatca cgtgagcgaagtatttacca tattacggtcagcagagcag tgacggttgatcttcgcttt tgttccagtttttcgatcca ttccgggatatatttgcctg atcggacggttaaggtcaac caactgtgcgaggatctctt gtgtagaaacgggatactgc ataatcgtgccgttaagcga gtgagcaatatcacgaccga ccatccgctctttcagtttg

Transcript	Probe sequences (5' to 3')

SodB	gtgcaggtaattcgaatgac agagcatctttagcatatgg tttccgcagaaatgtgcggt ttgccgtagtgatactcgat agtgacataagtctgatggt ctttaatcaggttgttcagg gatttaccttcaaacgcggt gctgcgaataatctcttcca tgttgaatacgccaccttca tggttccagacctgagctgc caggcagttccagtagaaag gttcgccaccggcgttcggt caaagtttcgacttttccag accagccaggtccagccaga cagtttgccatcgctgtttt gcgttagaggttgaaacgat atcggtggtcagcggagtac tcaacggtcagcagcggagt gtaataagcgtgttcccaga gacgtgcattgcgatagtcg cagaagtgctccagatagcc gaattcccagttcaccagcg

Supplementary Figures

Figure S1

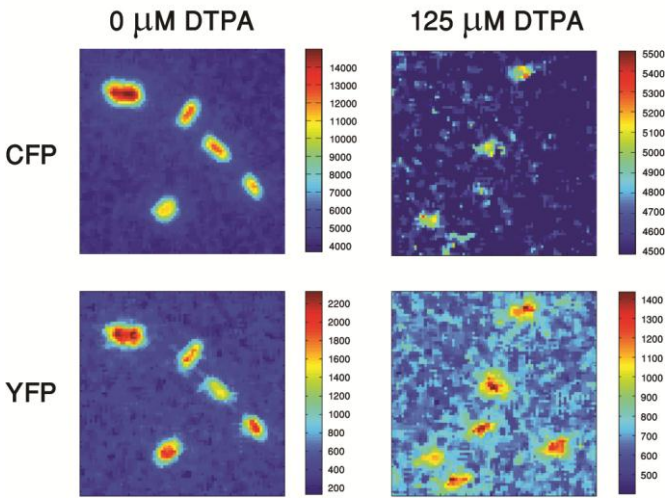

Figure S1 Representative images of *E.coli* dual reporter strain cells expressing SodB-CFP and FumA-YFP. The concentrations of FumA-YFP and SodB-CFP were measured in the same individual cells ~3.5 hours after exposure to 0 μM and 125 μM DTPA. The same field of view was imaged in both CFP and YFP wavelengths and the protein concentration was calculated from the images as described in the Supplementary Methods. The color bar represents the fluorescence intensity in arbitrary units.

Figure S2

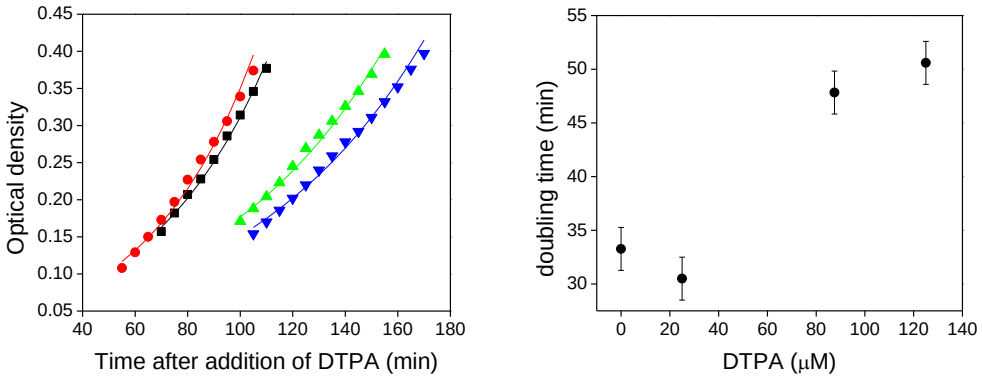

Figure S2 Effects of iron deprivation on growth curves. (Left panel) Optical density of cultures of MG1655 *E coli* strain as a function of time, after the addition of various concentrations of DTPA: 0 μM (red), 25 μM (black), 88 μM (green) and 125 μM (blue). The measurements were carried out on a plate reader at 37°C with shaking. Solid lines represent exponential fits to the data. (Right panel) Mean doubling time of cells as function of DTPA concentration. The data represent an average over two experimental runs carried out under the same conditions. Error bars denote standard errors. *E. coli* cell cultures (MG1655 strain) were grown overnight at 37°C in LB medium, then diluted 1:100 into fresh LB and allowed to reach an OD_{600} of 0.3-0.4. Cells were then further diluted 1:40 in LB containing various DTPA concentrations in a 96-well plate. Plates were maintained at 37°C with shaking throughout the experiments and optical density (OD_{600}) was measured as a function of time. Each experiment was repeated with similar results at least twice on different days. The slower growth may be due in part to recruitment of RNA polymerases by the strong RyhB promoter.

Figure S3

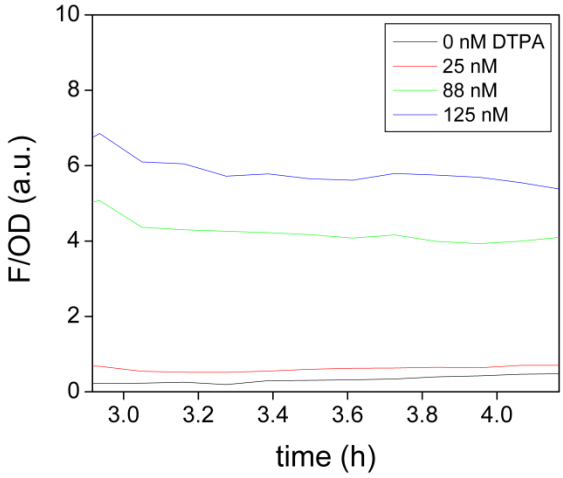

Figure S3 Evidence that adaptation to iron-poor conditions has been attained at the time at which measurements of noise are carried out. Measurements of fluorescence production normalized by optical density (OD) in cell cultures of MG1655 strain bearing reporter plasmids containing P_{ryhB} fusions to YFP as a function of time, following addition of the indicated iron chelator DTPA concentrations. All measurements were carried out under steady state conditions following the addition of the iron chelator DTPA, after the ensuing oscillations in gene expression have died out (5). MG1655 strain of *E coli* cell cultures bearing reporter plasmids containing P_{ryhB} fusions to YFP were grown overnight at 37°C in LB medium, then diluted 1:100 into fresh LB and allowed to reach an OD_{600} of 0.3-0.4. Cells were then further diluted 1:40 in LB containing various DTPA concentrations in a 96-well plate (Corning black with transparent bottom, Cat. no. 3651). Ensemble experiments were performed using Infinite 200 and Infinite 500 plate readers (Tecan Ltd). Plates were maintained at 37°C with shaking throughout the experiments and measured as a function of time. Each experiment was repeated with similar results at least twice on different days.

Figure S4

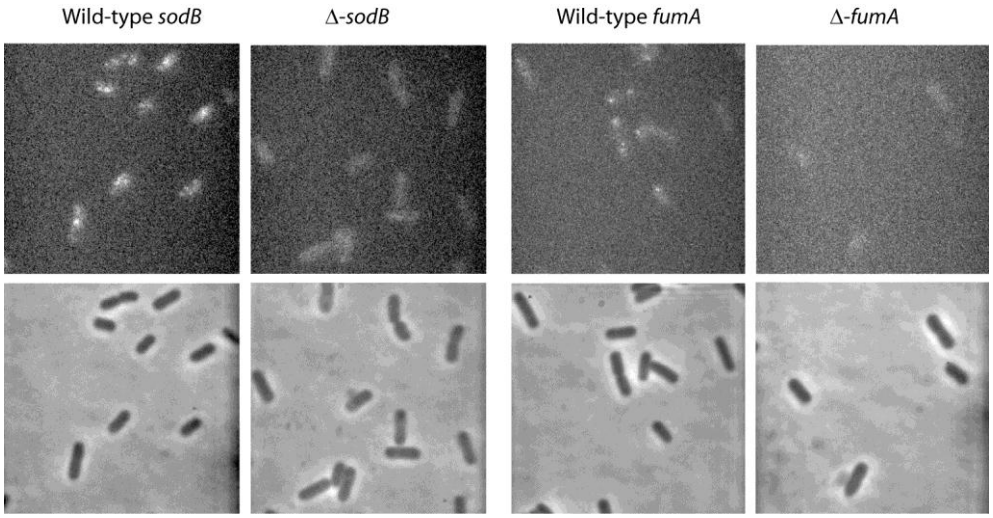

Figure S4 Quantitation of sodB and fumA transcript levels under iron-rich conditions. Top panels: typical fluorescence snapshots showing individual transcripts of either $mRNA_{sodB}$ and $mRNA_{fumA}$ in wild-type cells, visualized using smFISH techniques (see Materials and Methods), and the respective measurement of backgrounds in ΔsodB and ΔfumA cells. Bottom panels: corresponding phase contrast snapshots. The average number of transcripts under iron rich conditions are 4.9±0.6 for msodB and 1.2±0.2 for mfumA (mean ± standard error from seven experiments). Under iron starvation, a decrease in the small average for mfumA is in part balanced by an increase in the activity of its promoter (Supplementary Figure S5).

Figure S5

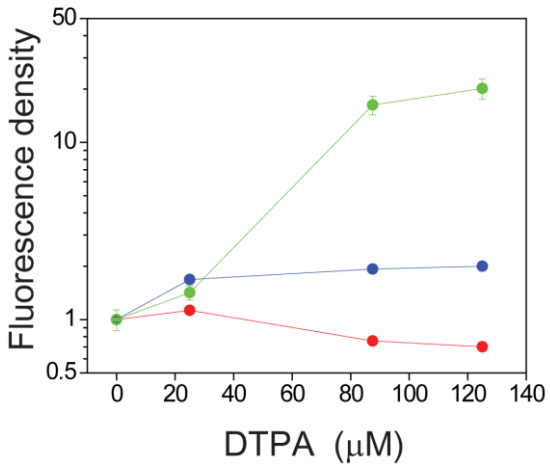

Figure S5 Effects of iron deprivation on the promoter activity of RyhB. Fold change in the mean fluorescence density, from an ensemble of cells bearing promoter fusion plasmids with either PsodB-YFP (red), PfumA-YFP (blue) or PryhB-YFP (green), ~3.5 hours after the addition of different concentrations of DTPA. The data represent an average over two experimental runs carried out under the same conditions as in Figure 2, each run consisting of ~500 cells. Error bars denote standard errors.

Figure S6

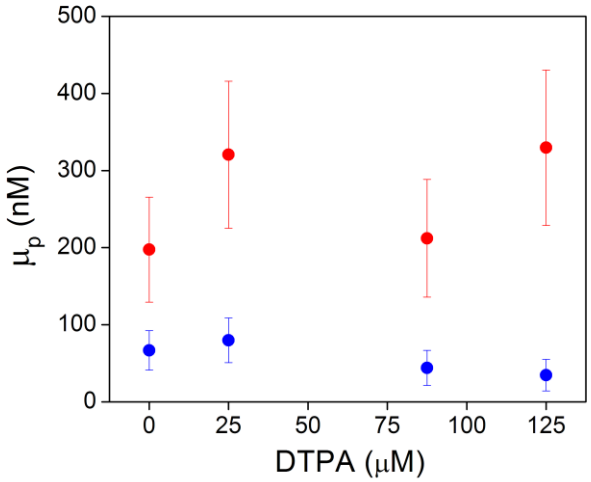

Figure S6 Independence of mean protein concentration of RyhB targets on iron deprivation in a ΔRyhB strain. Mean intracellular concentrations of SodB-CFP (red) and FumA-YFP (blue) as a function of DTPA concentration. Data points represent measurements over ~300 cells and error bars represent standard deviations.

Figure S7

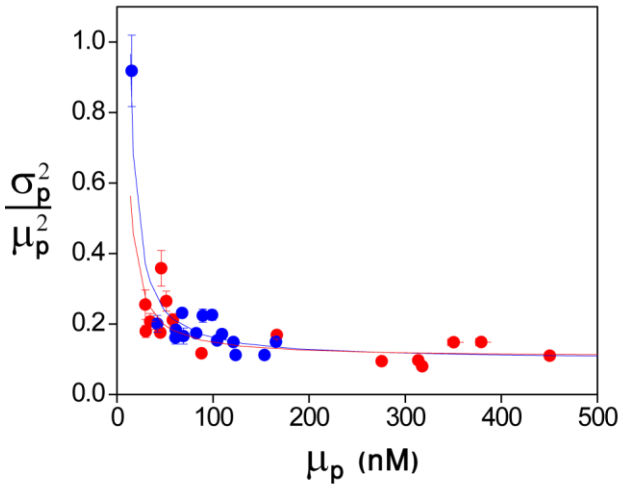

Figure S7 Dependence of total protein noise on the mean protein concentration. The total protein noise, quantified by the ratio σ_p^2/μ_p^2 between the variance σ_p^2 and the square of the mean protein number μ_p^2, is plotted as a function of μ_p both for SodB-CFP (red) and FumA-YFP (blue). The data correspond to those in Figure 3 in the main text. The lines correspond to the linear fits in Figure 3, namely, to $\sigma_p^2/\mu_p^2 = \left(\alpha + \beta/\mu_p\right)^2$, where the slopes α and intercepts β for both SodB-CFP and FumA-YFP being those of the linear fits in Figure 3. Irrespective of the extent of iron deprivation, all points fall well within the regime where extrinsic noise is dominant for other proteins in *E. coli* (4). Cells were exposed to different concentrations of DTPA ranging from 0 to 125 μM DTPA; the rightmost red and blue points correspond to 0 μM DTPA. Concentrations of DTPA above 125 μM were not used in order to avoid toxicity effects. Data were corrected for cell auto-fluorescence and were obtained from four independent experimental runs. Error bars represent standard errors derived from 1000 bootstrap samples of the data. Note that for DTPA=125 μM the cell doubling time is ~48 min in comparison to ~33 min for DTPA=0 μM, as determined from optical density measurements (see Figure S2).

Figure S8

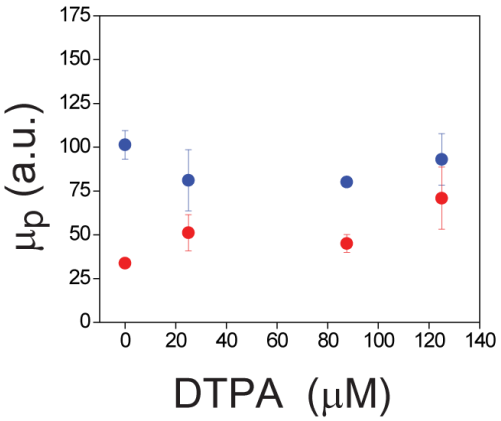

Figure S8 Mean fluorescence intensities from two reporters fused to identical promoters under different levels of iron deprivation. Fluorescence intensities of CFP and YFP reporters fused to different copies of the pLac promoter in the same cell, measured at different DTPA concentrations. Intensities were normalized both by cell volume and by the mean over the population. Mean fluorescence intensities of CFP (blue) and YFP (red) as a function of DTPA concentration. The data represent averages over two independent experimental runs, each consisting of ~1300 cells. Error bars represent standard errors.

Figure S9

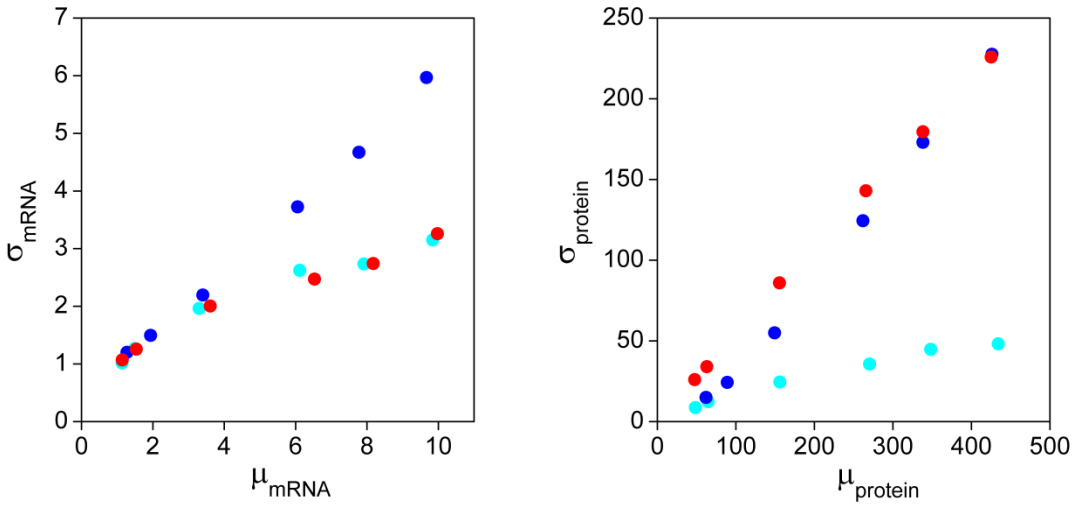

Figure S9 Stochastic simulation of gene expression in a network of two genes subject to down-regulation by a sRNA. Shown are the standard deviation of mRNA (left panel) and protein (right panel) versus the respective means across the population corresponding to one of the two target genes, in simulations carried out under the influence of different sources of noise: intrinsic noise alone (cyan); intrinsic noise plus extrinsic noise in transcription only (blue); intrinsic noise plus extrinsic noise in translation only (red). Extrinsic noise in transcription was introduced by multiplying the transcription rates of the two genes and the sRNA by a random number drawn from Gamma distribution. Extrinsic noise in translation was introduced by multiplying the translation rates of the genes' transcripts. The simulations were carried out in 1000 independent cells without transcriptional bursting and no explicit due to cell division. Simulation parameters are given in Supplementary Table S1. At the protein level, the standard deviation $\sigma_{protein}$ exhibits Poissonian behavior ($\propto \mu_p^{1/2}$) when intrinsic noise alone is the source of stochasticity. On the other hand, when extrinsic noise sources are included, the dependence of $\sigma_{protein}$ on μ_p is asymptotically linear (see Discussion in text). In comparison, at the mRNA level both intrinsic noise and extrinsic noise in translation yield Poissonian behavior, whereas extrinsic noise in transcription shows a linear behavior already at this stage.

Figure S10

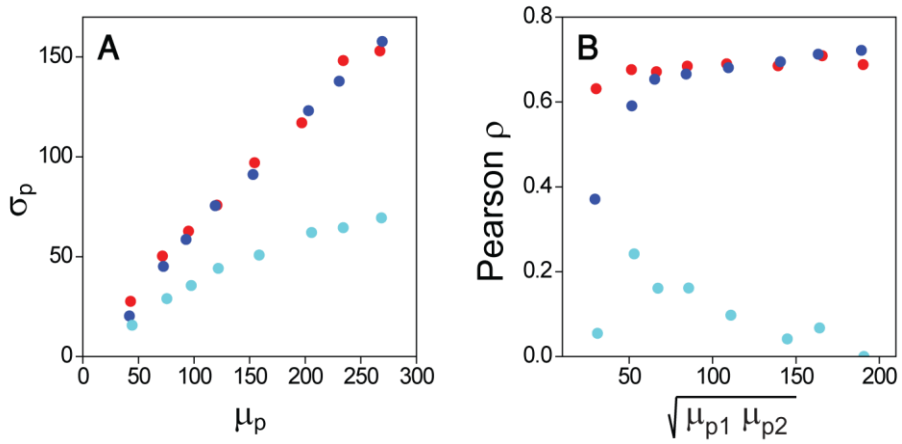

Figure S10 Stochastic simulation of a three target gene network. The first and second genes in these simulations represent *sodB* and *fumA* - the genes in our experiments. The third gene lumps together the effect of all other potential down-regulated RyhB targets, such as those shown in Table S3. (**A**) Standard deviation σ_p as function of the mean protein concentration μ_p of protein 1. (**B**) Pearson correlation coefficient ρ between the concentrations of proteins 1 and 2 as function of the geometric average of their mean concentrations. sRNA levels were varied between simulation points to represent variation in iron deprivation levels by DTPA. As with the simulations of two targets, extrinsic noise was considered in: transcription only (all transcription rates in each cell were multiplied by a random number drawn from Gamma distribution) (blue); translation only - translation rates in each cell were multiplied by the same random number (red). Results of simulations including intrinsic noise alone are also shown for reference (cyan). As with a network including two targets only, σ_p is linear with μ_p for both extrinsic noise sources in transcription and translation. Note that the third target competes effectively for the sRNA, preventing μ_p (and σ_p) from reaching small values as in the case of two genes (Figure 6). The Pearson correlation shows similar trends to those observed in simulations without competitor. The transcription rates of targets 1 and 2 were 1 and 0.5 respectively, whereas that of gene 3, 15. The affinities of targets 1, 2 and 3 for the sRNA were taken to be 0.02, 0.02 and 0.005 respectively.

Figure S11

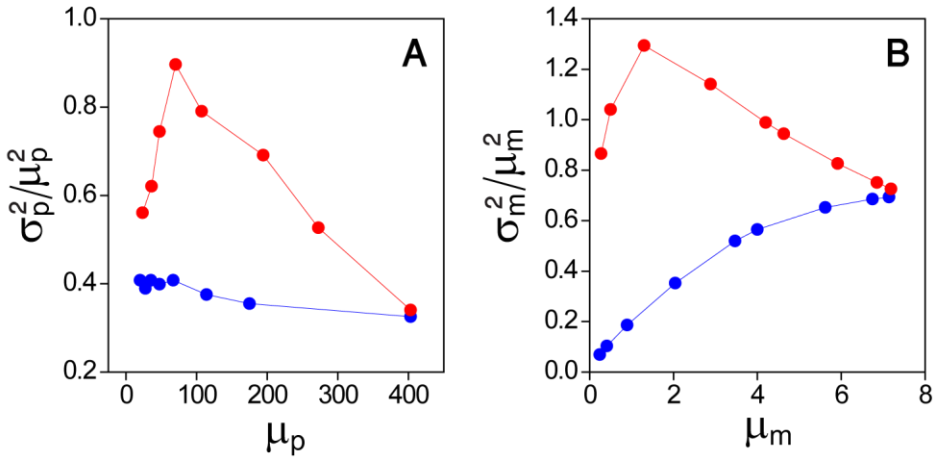

Figure S11 Effects of the abolishment of the threshold-linear relationship on protein noise when sRNA production is only subject to intrinsic noise while mRNA production is subject to transcriptional extrinsic noise. (A) Protein noise as function of the protein mean concentration from stochastic simulations in which sRNA production is only subject to intrinsic fluctuations while mRNA production is also subject to transcriptional extrinsic sources. Simulations were carried out both when the sRNA and transcripts undergo stoichiometric degradation (red), or when the sRNA acts catalytically promoting mRNA degradation without being degraded as a result of the interaction (blue). Catalytic degradation effectively abolishes the threshold-linear expression relationship (1). (B) Transcript noise obtained from an analytical solution of steady-state equations of mRNA levels (6). Extrinsic noise has been added by multiplying transcription rates by 10,000 numbers drawn from a Gamma distribution, and then calculating the steady-state concentrations of the mRNA. The blue trace corresponds to an I1-FFL formed by transcriptional extrinsic noise affecting directly the expression of targets and indirectly via a sRNA, while the red trace corresponds to extrinsic noise affecting only mRNA transcription rates. Note that intrinsic noise sources do not play a role since they do not affect sRNA and mRNA production. The simulation parameters used to calculate the plots in this panel are: 1.5 for transcription rates; 0.02 for the mRNA-sRNA binding coefficient; the Gamma distribution had a variance of 0.5 and mean 1; 0.2 and 0.04 were the mRNA and sRNA degradation rates respectively.

Figure S12

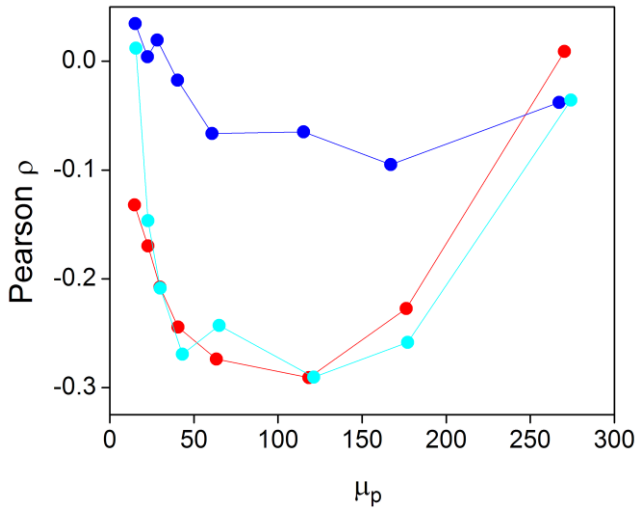

Figure S12 Pearson correlation ρ between sRNA and target transcript levels under different types of noise sources. The positive correlation of sRNA and its target mRNAs induced by transcriptional extrinsic noise is largely cancelled out by the stoichiometric degradation of both, yielding slightly negative values for ρ (blue). In contrast, under translational extrinsic noise (red), which affects neither the sRNA nor its target mRNAs, the correlation is significantly more negative, since large levels of sRNA production lead to small target transcript levels and vice versa. Given that neither the sRNA nor the target transcripts are affected by translational extrinsic noise, the effect is similar to that of purely intrinsic noise (cyan).

Figure S13

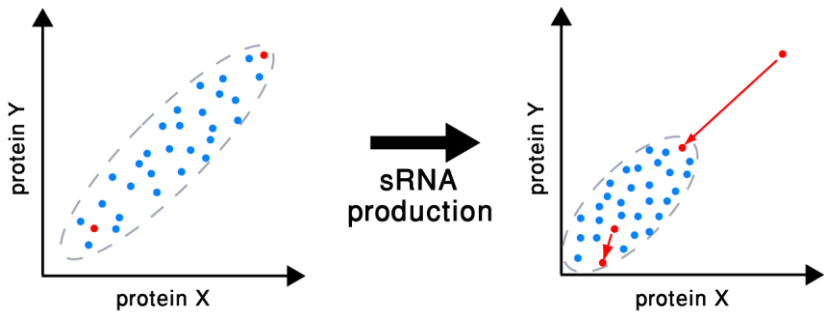

Figure S13 Mechanism for the reduction of correlation in the expression of coordinately, down-regulated target proteins, under transcriptional extrinsic noise dominance. Scatter plot of cells expressing proteins X, and Y when transcriptional extrinsic noise dominates their variability. It is assumed that translation is proportional to the amount of the corresponding transcripts. When sRNA production is elicited, cells having a large concentration of $mRNA_Y$ will have both large concentrations of $mRNA_X$ and sRNA, leading to a large reduction in X and Y amounts (large red arrow). The reduction in protein concentrations is smaller for cells having smaller amounts of X and Y from the outset (small red arrow). Consequently, a cigar-shaped cluster of cells will become more circular when sRNA is produced, thereby reducing the Pearson correlation between both target proteins. This effect will be enhanced by the expected increase in intrinsic noise when the number of mRNA molecules becomes small by sRNA-induced degradation. Even if a peak in intrinsic noise is present as theoretical calculations indicate (6), it is narrow. An increase in intrinsic noise broadens the spatial extent of the cluster in the direction perpendicular to the main diagonal.

Supplementary Methods

Bacteria and culture conditions

All strains used in this study were derived from *E. coli* MG1655. Bacteria were grown in Luria-Bertani (LB) medium or on LB agar plates. Asnecessary, chloramphenicol (Cm), kanamycin (Km) and tetracycline (Tc) were added, to final concentrations of 15, 15 and 3 µg/ml, respectively.

Construction of *E. coli* reporter strains

The *sodB::cfp* and *fumA::yfp* genes bear a translational *cfp*-fusion to the chromosomal *sodB* allele or *yfp*-fusion to the chromosomal *fumA* allele. Recombineering (recombination-mediated genetic engineering) was used to construct a chromosomal *sodB-cfp* reporter strain. Subsequently a genomic *fumA-yfp* fusion was constructed in the *E. coli sodB-cfp* genetic background. TripleMaster DNApolymerase (Eppendorf) was used for PCR. DNA fragments were excised and purified with the Qiagen Qiaquick extraction kit; DNA sequencing was performed at GATC biotech.

FRT-flanked Cm^R cassette A006 (Gene Bridges) was PCR-amplified using primers *sodB* PCR1 up/down (Supplementary Table S2) and inserted into pZE12 by Red/ET recombination, yielding $pCFPCm^R$. The resulting *cfp* FRT-Cm^R-FRT stretch from pCFP-Cm^R was PCR-amplified with primers *sodB* PCR2 up/down (Supplementary Table S2). Thereby a 36 bp 5´ linker sequence and flanking arms (50 bp) homologous to the 3´end of *sodB* and the sodB-*ydh*P intergenic regionwere attached to the linear insertion construct (2427 bp).

A 1144 bp DNA fragment encoding for the linker sequence (the stop codon that was replaced by the encoding for amino acid linker GSAGSAAGSGEF) and yellow fluorescent protein was synthesized by GENEART. This fragment features terminal sequence overlaps with the 3´end of *fumA* (107 bp) and the 5´end of FRT-flanked Km^R cassette A002 from GeneBridges (283 bp). In turn resistance cassette A002, amplified with primers *fumA* PCR up/down (Supplementary Table S2) features a 3´ homology arm (70 bp) specific for the *fumA-fumC* intergenic region.

Red/ET recombineering was performed as described by Gene Bridges (http://www.genebridges.com). In brief, 1.4 ml of Red/ET proficient cultures were aerobically grown at 30°C to an OD_{650}nm of ~0.3. Expression of Red genes encoded by pRed/ET (Gene Bridges) was induced by adding 50 µl of 10% (w/v) L-arabinose followed by a temperature increase to 37°C. After 1h of incubation the cells were washed twice with ice cold 10% (v/v) 2 glycerol and electroporated with i) 500 ng of linker-*cfp* FRT-Cm^R-FRT construct (for s*odB-cfp* reporter strain) and ii) 250 ng of synthetic linker-yfp fragment and the corresponding FRT-flanked Km^R cassette (for double reporter strain) at 1.35 kV, 10µF, 600Ω using Eppendorf electroporator 2510. Subsequently the cells were resuspended in 1 ml ice-cold LB-medium and aerobically grown at 37°C for 1h. Plates supplemented with either Cm or Km were used to select for recombinants. Colony-PCR was performed to check for correct fragment insertion by using one primer annealing to the insert (i.e. *cfp, yfp*) and the other to flanking genomic sequence. The products of Red/ET cloning, as described above, include selectable CmR and KmR genes, respectively. The flanking FRT sites allowed for the successive removal of the markers by Flp recombinase, leaving a single FRT site (34 bp) at the point of DNA manipulation. Therefore Flp-encoding plasmid 706-FLP (A103, Gene Bridges) was introduced into the Red/ET recombinants by electroporation. Tc^R transformants obtained at 30°C were used to inoculate 1 ml LB cultures,

which were incubated at 30°C for 3 h. Flp activity was induced by a temperature increase to 37°C. Single colonies obtained on LB plates at 37°C were subsequently screened for Cm- or Km-sensitive phenotypes. Loss of the resistance markers, correct insertion into the genome and integrity of the *sodB-cfp* and *fumAyfp* gene constructs were demonstrated by the size and sequence of PCR products amplified from genomic DNA with primers sodB up/down and fumA up/down.

Production from the native promoters of *ryhB, sodB* and *fumA*

Production from the native promoters of *ryhB, sodB* and *fumA* was monitored by low copy number plasmids which encoded for YFP. P_{ryhB}-YFP, P_{sodB}-YFP and P_{fumA}-YFP plasmids were constructed using the low copy plasmid pBAD-24 as backbone (7).The promoter region was PCR-amplified from the bacterial genome using *E. coli* MG1655 cells using the SodB PCR3 up/down primers for *SodB* or FumA PCR4 up/down primers for *fumA* (Supplementary Table S2). The resulting insert fragments were cloned into the backbone plasmid using the restriction enzymes AgeI and EcoRI. The gene for YFP was PCR amplified from the pZA32 plasmid (from M. Elowitz) and cloned into the backbone plasmid downstream of the *sodB* and *fumA* promoter region. Correct insertions were verified by DNA sequencing. P_{sodB}-YFP and P_{fumA}-YFP plasmids were transformed into MG1655 *E. coli.* Similarly, P_{ryhB}-YFP was constructed as described previously (5).

Strains bearing dual chromosomal *sodB* genes

We have prepared two strains bearing dual chromosomal copies of the *sodB* gene. In the first strain the *sodB-yfp* gene together with its native promoter and all its regulatory elements was inserted at the *lac* operon. The *sodB* gene and its upstream regulatory region were amplified from between *E. coli* coordinates 1,733,272-1,733,980 with primers having 50bp segments at their 5' ends that are homologous to either *lacI* or *lacZ*. This amplified cassette with flanking homology was electroporated into strain NC397, which is chloramphenicol resistant and sucrose sensitive as described and described previously (See Supplementary Materials for Svenningsen et al (8)). Using standard recombineering procedures a *lac* operon segment (from *E. coli* coordinates 365,501 to 366,643) was replaced with the *sodB* cassette by selecting for sucrose resistant and Cm^S colonies. These colonies were purified, verified by PCR and their sequence determined. The *yfp-FRT-kan-FRT* cassette was amplified from the MG1655 strain bearing *fumA-yfp-FRT-Kan-FRT* (Gene Bridges) with hybrid primers that had 50bp of homology at the 5' end to either *sodB* or *lacZ*. This cassette was electroporated into the above strain, selecting for Kan^R recombinants in which the *yfp* cassette was fused to *sodB*; such that *yfp* is fused in frame to *sodB* as in the native location. Isolates were purified then verified by PCR and sequence analysis. This *sodB-yfp-kan* recombinant at *lac* was moved into a MG1655 strain bearing *sodB-cfp* by standard P1 transduction selecting for Kan^R. In a final step the purified isolates were transformed with pCP20, a Cm^R pSC101^{ts} plasmid that expresses the Flp recombinase gene for removing the *kan* from between *frt* sites. This plasmid was subsequently cured out at 42° with isolation of a kanamycin and chloramphenicol sensitive colony.

In the second strain we selected a rare, natural duplication of the *sodB-cfp* gene within the *ribC* gene, less than 8000 bp apart from the native location of the *sodB* gene, and then substituted the *cfp* for *yfp*. The *yfp-FRT-kan-FRT* cassette was amplified from the MG1655 strain

bearing *fumA-yfp-FRT-Kan-FRT* with hybrid primers that had 50bp of homology at the 5' end to either *sodB* or the downstream region. This cassette was recombined into strain DY378 using standard recombineering protocols and kanamycin resistant colonies were purified, verified by PCR and their sequence analyzed. A P1 lysate was prepared on the strain for transduction into a tandem diploid. A MG1655 strain bearing *sodB-cfp* at its native site was transformed with pSIM18 to provide the Red recombination functions. The essential *ribC* gene near *sodB* was targeted to replace its open reading frame with a *tet* cassette. Hybrid primers contained 50 bp segments at their 5' ends that are homologous to each end of the *ribC* coding frame. This cassette was recombined into the strain using standard recombineering procedures and selecting for Tet^R colonies, which were purified on LB tet and analyzed by PCR using primers that flank the *ribC* gene. When essential genes are targeted for recombination, the only recombinants to survive are those rare cells already present in the original population that were diploid for the region of the essential gene (9). By maintaining selection for Tet the diploidy is maintained in the culture. Constructs were verified by PCR analysis using primers outside *ribC*, which generate two distinct bands on a gel: a 693bp band corresponding to the *ribC* gene and a 1426bp band corresponding to the *tet* replacement of *ribC*. In all subsequent work strains were grown in the presence of tetracycline to maintain the tandem diploid. The diploid region is unable to be transduced from one strain to another indicating that it is probably more than 100kbp in length. A P1 lysate made from the *sodB-yfp-kan* strain was used to transduce into the tandem diploid strain, selecting for Tet^R Kan^R. Isolates were purified and analyzed by PCR using sets of specific primers to confirm the presence of both a *yfp* and a *cfp* gene fused to their respective copy of *sodB*. In a final step the purified isolates were transformed with pCP20, a Cm^R $pSC101^{ts}$ plasmid that expresses the Flp recombinase gene for removing the *kan* from between *frt* sites. This region will remain duplicated as long as the strain is grown in the presence of tetracycline. This duplications strain was transformed with pSIM18 and by recombineering one copy of cfp was replaced with yfp-kan. In a final step the kan cassette was removed from the strain.

Strain bearing *sodB::cfp* and *fumA::yfp* genes and a *ryhB* deleted gene

The strain MG1655 bearing *fumA-yfp-FRT-Kan-FRT* (Gene Bridges) was transformed with pSIM18. The tetA gene was amplified with hybrid primers (given in Supplementary Table S2) that contained homology to the upstream and downstream regions of the target gene *ryhB*, which was replaced by the tetA cassette using standard recombineering techniques (10). After confirmation of the replacement, the pSIM18 plasmid temperature sensitive for replication was cured from the strain by growth at 42°. The tetA-resistant colonies were purified, verified by PCR and their sequence was analyzed.

Measurement of msodB and mfumA transcripts using single-molecule fluorescence in situ hybridization (smFISH)

The procedures we follow are based on (2).

Probe design and labeling

DNA oligonucleotide probes of SodB and FumaA were designed using the Stellaris RNA probe FISH designer (https://secure.biosearchtech.com/stellarisdesigner/). The Stellaris™ FISH probes were tagged with Fluorescein Dye (Fluor® Red 590 Dye). Sequences of smFISH probes are given in the Supplementary Table S4. The probes were dissolved in 10mM Tris-HCl 1mM EDTA (pH 8.0) to create a probe stock at a total oligo concentration of 25 µM. The tube was wrapped in aluminum foil and stored at -20 °C.

Sample fixation and permeabilization

An overnight culture of SodB and FumA deleted *E coli* strains from the KEIO collection (11) and MG1655 *E coli* strain, were diluted 100 into 4 ml of LB medium. The cultures were incubated at 37 °C with shaking. When OD600 of the culture reached 0.3–0.4, cells were pelleted by centrifugation (5 minutes, 4500×g, 4 °C). The supernatant was removed and the cells were resuspended in 1 ml freshly prepared 3.7% formaldehyde in 1× PBS (diluted from 10× PBS). The cells were then transferred to a microcentrifuge tube and mixed on a rotator at room temperature for 30 minutes. The cells were pelleted by centrifugation (5 minutes, 4500×g). The supernatant was removed and the cells were washed in 1 ml 1× PBS twice (i.e. resuspended in 1 ml 1× PBS, centrifuged at 3500×g for 7 minutes, and supernatant removed). The cells were resuspended in 300 µl water, and then 350 µl of 100% ethanol was added and mixed twice to get to a final concentration of 70% ethanol. The cells were left at room temperature with mixing on a rotator for at least 1 hour (or alternatively, at 4 °C for at least a week) to permeabilize the cell membrane.

Hybridization

After permeabilization, cells were centrifuged (7 minutes, 750×g) and the supernatant was removed. The cells were resuspended in 1 ml of 40% wash solution (see below) and the tube was left standing for a few minutes. An aliquot of 40% hybridization solution (see below) was warmed to room temperature and 50 µl was added to a microcentrifuge tube. 3 µl of a 10-fold diluted probe solution was added to the hybridization solution and mixed well. The cells were then centrifuged (7 minutes, 750×g) and the supernatant was removed. The cells were resuspended in the hybridization solution with probes and left at 30 °C overnight. Hybridized samples could be stored at 4 °C for at least 6 months. 10 ml of 40% wash solution contains 4 g of formamide and 1 ml of 20× SSC. 10 ml of 40% hybridization solution contains 1 g of dextran sulfate 4 g of formamide, 10 mg of E. coli tRNA, 1 ml of 20× SSC, 40 µl of 50 mg/ml BSA, and 100 µl of 200 mM ribonucleoside vanadyl complex. The solution was filter sterilized, aliquoted, and stored at -20 °C.

Washing

10 µl of hybridized sample was transferred to a microcentrifuge tube. The rest was stored at 4 °C. 200 µl of 40% wash solution was added to the tube and mixed well. Cells were pelleted by centrifugation (7 minutes, 750×g) and the supernatant was removed. The cells were washed again in 1ml of 40% wash solution, centrifuged at 750×g for 7 minutes, supernatant removed, and cells were resuspended in 50 µl of 2× SSC and imaged under the microscope.

Transcript visualization

An agarose gel pad (1.5%) in SSCx2 was made on a coverslip and 5 µl of sample was pipetted onto the pad and a #0 mm coverslip was placed on top of the agarose gel pad. The sample was imaged under our microscope using a 100× N.A. 1.3 oil immersion phase contrast objective (Zeiss Neoplan 100x 1.3 phase contrast) and our cooled camera. The objective lens was mounted on a Mipos100 piezo controller (Piezosystem Jena). The microscope and camera were controlled using a custom made program in Matlab (MathWorks). The filters used to image the cells are FF01-503/572-25 for excitation, FF444/520/590-Di01 for dichroic mirror and FF01-628/32 for emission (Semrock). A phase contrast image was acquired followed by a z-stack of 17 slices and 250 nm spacing of fluorescent images with 2s integration time of each slice. Each sample was imaged at multiple locations to get a total of at least 500 cells.

Cell recognition

Cell recognition was performed on phase contrast images of cells using a custom made program written in Matlab. The program applies edge detection and other morphological operations, using the MATLAB Image Processing Toolbox. The output was checked and corrected manually and parameters such position, length and area of each cell could be extracted.

Spot recognition

A spot recognition program developed in our lab, based on published procedures (2) was used to automatically identify and quantify localized fluorescence signals. A Gaussian filter was first applied to smooth out noise, and spots were recognized by the presence of a local maximum in both x- and y-directions. This was done at each z-position in the stack of images, and each spot was quantified at the z-position where it had the highest fluorescence intensity (where the spot is in focus).

Estimating mRNA numbers

A fluorescence spot could consist of multiple mRNAs in close proximity. The integrated intensity arising from a single mRNA needed to be estimated for each smFISH experiment so that fluorescence intensities could be normalized to give the absolute number of mRNAs. The typical intensity of "false positives" in an experiment was first estimated from the histogram of individual spot intensities of a negative control (*E. coli* strains Δ*sodB* or Δ*fumA*). Histograms of individual spot intensities from relatively low expression samples (exposed to 125 µM DTPA) were then examined. Because most spots in these samples were expected to contain a single mRNA, the first peak that emerged above the false positive range in each of these histograms served as an estimate for the intensity of a single mRNA. The mean intensity of the first peaks from multiple such histograms was taken as the single mRNA intensity for that particular experiment. The sum of intensities of all spots in each cell was then normalized to give absolute number of mRNAs.

Measuring SodB-CFP and FumA-YFP concentration in live cells

Experimental setup

Filters (Semrock, USA) FF01-434/17 and FF01-479/40 are the CFP channel excitation and emission filters, respectively. Filters FF01-504/12 and FF01-535/22 are the YFP channel

excitation and emission filters, respectively. The channels have a common dichroic mirror FF444_520_590-Di01 and the emission and excitation channels are switched using filter wheels. The objective lens is mounted on a Mipos100 piezo controller (Piezosystem Jena, Germany) and equipped with an objective temperature controller (Pecon, Germany) set for 37 ^{o}C during the measurments. Images were obtained using an iXon EMCCD (Andor Technology, Northern Ireland). Both phase contrast and fluorescence images were captured. Each bacterial cell was automatically marked for total fluorescence as well as cell area and length data using a home-built MATLAB application.

Image acquisition

Image acquisition was performed using a custom MATLAB (MathWorks) application. The acquisition begins with an autofocus routine based on maximum contrast on the phase contrast image during Z-scanning using the objective piezo mount. Once optimum focus is found, a YFP fluorescent image is taken followed by a dark image (no illumination). Then the CFP fluorescent image is taken followed by a dark image. The integration time of the fluorescent images is 2 seconds for both channels.

Image processing

All image processing and data analysis were performed using MATLAB (MathWorks). Cell recognition was performed on phase contrast images of cells using a program developed in our lab. The program applies morphological operations, using the MATLAB image processing toolbox. The program's output was checked manually in all experiments and corrected for errors in recognition. Fluorescence images were corrected as follows: Each fluorescent image acquisition was followed by the acquisition of a dark image using the same parameters as the fluorescent image. The dark image was then subtracted from the fluorescent image. To compensate for illumination pattern, we measured it using fluorescein, and the fluorescent image was then divided by the fluorescein correction image to yield a flattened image. To correct for background fluorescence, the background fluorescence from the vicinity of each cell was measured and subtracted from that cell.

Correction for cell auto-fluorescence

For the calculation of the standard deviation as a function of the mean protein concentration in Figure 4 and the Pearson correlation in Figure 6 we had to correct for the cells auto-fluorescence. We took images of wild-type MG1655 and analyzed their fluorescence statistics using the relation: $F = AF + S$ where F is the measured fluorescence, AF is the measured auto-fluorescence of the wild-type cells and S is the fluorescence from the fluorescent proteins. Since S and AF are independent, we can write: $\sigma_S^2 = \sigma_F^2 - \sigma_{AF}^2$ and $\mu_S = \mu_F - \mu_{AF}$.

Computation of fluorescence concentrations

Total fluorescence levels from isolated cells in the field of view were calibrated in terms of protein numbers by using a method based on the binomial statistics of protein partition as cells divide (12). Then concentrations of both SodB-CFP and FumA-YFP were calculated by dividing the number of each protein by the cell volume, calculated as 2/3*(cell area)*(cell width), following previous methods (4).

Calculation of extrinsic noise from the normalized correlation function of SodB-CFP and FumA-YFP

Under iron-rich conditions in which the expressions of SodB-CFP and FumA-YFP are independent, the normalized correlation between their concentrations provides a measurement of the global extrinsic noise η_{ext}^2 (4):

$$corr(\text{SodB-CFP}, \text{FumA-YFP}) = \frac{\langle \text{SodB-CFP} \times \text{FumA-YFP} \rangle}{\langle \text{SodB-CFP} \rangle \langle \text{FumA-YFP} \rangle} = 1 + \eta_{ext}^2$$

Calculation of Pearson correlation

The Pearson correlation coefficient (Figure 6B) is calculated as:

$$\rho = \frac{\langle (c - \mu_c)(y - \mu_y) \rangle}{\sigma_c \sigma_y}$$

With c and y the concentrations of SodB-CFP and FumA-YFP respectively and μ and σ are the corresponding mean and standard deviation. Error bars in ρ were calculated using 1000 bootstrap samplings of the data.

Stochastic simulations of two genes whose expression is controlled by a sRNA

We simulated the stochastic dynamics of a network consisting of two genes encoding for proteins and a third gene encoding for a sRNA that promotes the degradation of the other two transcripts. We utilized the Gillespie algorithm (13) to obtain full time traces of all the molecules involved and studied how different transcription rates of the sRNA affect the distribution of the two proteins synthesized and their correlation to each other. For simplicity the two genes in our simulation were assumed to have equal rates of transcription and translation, and their transcripts were assumed to have the same affinity to the sRNA.

To incorporate extrinsic noise, we drew random numbers from a Gamma distribution, one number for each cell, and multiplied the three transcription rates (or two translation rates) of each cell by the same number. The Gamma distribution was taken with mean equal to 1, in order to maintain the average rates intact and with variance that matches experimental results. The results of simulations without extrinsic noise are also shown for reference.

For each noise model (intrinsic only, extrinsic in transcription or extrinsic in translation), we kept all parameters constant and only varied the sRNA transcription rate, in order to mimic the effect of different DTPA levels. We simulated 300 minutes time traces (equivalent to 10 cell generations), in order to enable the simulation to reach steady state. We repeated the simulation 1000 times independently in order to gain population statistics. Molecule statistics were calculated based on the finite number of molecules at each trial, in order to reflect a population snapshot taken at an arbitrary time.

In our basic simulation transcription was assumed to occur at a constant rate, rather than in bursts. As an additional option, we also included transcriptional bursting, which increased the intrinsic noise significantly, but still did not change the trends in our results. Bursts

were added following the two-state model (2). In this model a gene can be in either an "on" or an "off" state and transit between the two with rates k_{off} and k_{on}. When in the "on" state, the gene is transcribed at a rate k_{tx}. So *et al* found that expression level is modulated mainly by k_{off}. We therefore took k_{on} and k_{tx} to be constant and gene-independent, and varied k_{off} only. Note that the different values of k_{off1} and k_{off2} were chosen so that the promoter activities of the two target genes, given by $PA = k_{tx}\left(k_{on}/\left(k_{on} + k_{off}\right)\right)$, differ by a factor of two, similar to the ratio between the steady state average concentrations of msodB and mfumA transcripts (Supplementary Figure S4). Cell division was included in the simulations by assuming that at the end of each cell cycle all the molecules are split with binomial distribution between the two daughter cells and only one of the cells is picked up to continue the simulation with. The protein numbers were sampled at a random time along the last generation and normalized by a number between 0.5 and 1, which is proportional to the time since last division (0.5 for cells sampled right after division and 1 for cells sampled just before division). The random sampling and normalization were performed in order to eliminate effects resulting from sampling time along the cell cycle. This however, had only a minor effect on our results and did not change our general conclusions.

Simplifications made here include: assuming independence of cell generation times and variability of rates on the sRNA level, neglecting the effect of additional sRNA targets, taking the common noise factor to be constant throughout each simulated trajectory. The last assumption is expected to bring about an increase in the simulated Pearson correlation between the proteins, compared to the correlation in reality.

An example of simulation results at both RNA and protein level with extrinsic noise at either transcription or translation is shown in Supplementary Figure S9.

Specifically, our simulation consisted of the following list of reactions:

$$on_1 \xrightarrow{k_{tx}} m_1 + on_1 \quad (1a)$$

$$on_2 \xrightarrow{k_{tx}} m_2 + on_2 \quad (1b)$$

$$on_R \xrightarrow{k_{tx}} R + on_R \quad (1c)$$

$$m_1 + R \xrightarrow{k_4} \emptyset \quad (1d)$$

$$m_2 + R \xrightarrow{k_5} \emptyset \quad (1e)$$

$$m_1 \xrightarrow{k_6} m1 + p_1 \quad (1f)$$

$$m_2 \xrightarrow{k_7} m_2 + p_2 \quad (1g)$$

$$m_1 \xrightarrow{k_8} \emptyset \quad (1h)$$

$$m_2 \xrightarrow{k_9} \emptyset \quad (1i)$$

$$R \xrightarrow{k_{10}} \emptyset \quad (1j)$$

$$p_1 \xrightarrow{k_{11}} \emptyset \quad (1k)$$

$$p_2 \xrightarrow{k_{12}} \emptyset \quad (1l)$$

$$on_1 \xrightarrow{k_{off1}} off_1 \quad (1m)$$

$$off_1 \xrightarrow{k_{on}} on_1 \quad (1n)$$

$$on_2 \xrightarrow{k_{off2}} off_2 \quad (1o)$$

$$off_2 \xrightarrow{k_{on}} on_2 \quad (1p)$$

$$on_R \xrightarrow{k_{offR}} off_R \quad (1q)$$

$$off_R \xrightarrow{k_{on}} on_R \quad (1r)$$

where $m_{1,2}$ denote the two mRNAs, R denotes the sRNA and $p_{1,2}$ denote the proteins. Reactions a-c describe transcription, d-e destructive interaction between sRNA and mRNA, f-g describe protein translation, h-l describe molecule decay, m-r describe transcriptional bursting. If explicit cell division was incorporated (as explained above) reactions k-l were not used. Similarly, reactions m-r were not applied, if bursting was not included in the simulation.

The following simplifying assumptions were made in the simulations. Fluctuations in different upstream factors to which expression from the sodB and fumA genes are subject, were not included in the simulations. On one hand our experiments show that iron deprivation leads to an increase in cell doubling time. On the other, it is known that this is accompanied by a decrease in the mean number of RNA polymerase and ribosome numbers (14). While this decrease lowers the protein production capacity, this is partially compensated by the increase in cell doubling time, allowing for more proteins to accumulate. We have neglected both effects in the simulations, in accordance with our pLac experiments in which the measured extrinsic noise is not significantly changed with iron deprivation. Lastly, extrinsic noise sources were taken to be constant throughout each simulated trajectory, whereas in reality, RNA polymerase and ribosome numbers are prone to changes through cell division, fluctuating with timescales similar to the cell cycle (12). These simplifying assumptions may account for the discrepancy between the values $\rho \sim 0.7$ obtained in the simulations, under conditions in which the rate of sRNA synthesis is small and that observed in the experiments $\rho \sim 0.5$. Note that the reduction of the Pearson correlation by a factor of nearly two over the range of DTPA of our experiments most probably reflects the presence of both extrinsic noise in transcription and translation.

Initial conditions for the simulations were chosen as steady-state conditions of equations SI-2 (for proteins) and SI-5 (for mRNA and sRNA) in the Supporting Information of Ref. (6), in order to arrive as fast as possible to the steady-state. Other choices of initial conditions yield similar results, but with longer running times.

Supplementary Text

Intrinsic noise dominates phenotypic variability for small values of the mean protein concentration μ_p .

In measurements (Figure 3, main text) and simulations (Figure 6A, main text) presented in the main text, the standard deviation of protein distributions σ_p was observed to depend linearly on the mean μ_p, due to extrinsic noise. However straight line fits to these data did not intercept the origin. Here we argue that this is due to additional intrinsic noise, whose behavior is Poissonian. Assuming intrinsic and extrinsic noise sources are uncorrelated, their variances add up to yield the total variance:

$$\sigma_{tot}^2 = \sigma_{int}^2 + \sigma_{ext}^2$$

Since intrinsic noise is characterized by Poissonian statistics, $\sigma_{int} = k_i \mu_p^{1/2}$ whereas for large values of the mean μ_p, $\sigma_{ext} = k_e \mu_p$. Then for $(k_i/k_e)^2 \ll \mu_p$ one obtains to first order:

$$\sigma_{tot} = k_e \mu_p \sqrt{1 + \left(\frac{k_i}{k_e}\right)^2 \frac{1}{\mu_p}} \approx k_e \mu_p + \frac{{k_i}^2}{2k_e}$$

A straight line fit to data for which the second term in parenthesis is small (large μ_p) will therefore cross the σ_p axis at a non-zero, positive value ${\sigma_{tot}}^*$ given in this case by:

$${\sigma_{tot}}^* = \frac{{k_i}^2}{2k_e}$$

a value that is independent of μ_p. Using the values of the slopes obtained from the linear fits to the experimental data shown in Figure 4 in the main text as well as the values of the intercepts, we obtained $(k_i/k_e)^2 \sim 40$ nM, which is consistent with the deviation from linearity observed in our simulations (Figure 6A, inset, main text)

Extrinsic noise sources can produce a linear dependence of σ_p on μ_p.

We now discuss cases in which extrinsic noise sources can produce a linear dependence of σ_p on μ_p as we observe in our experiments. In a simple model of gene expression, the steady-state mean protein number $\bar{p}$ in a cell for a gene transcribed and translated with rates α_m and α_p respectively, and whose transcript and protein are degraded by first-order kinetics with rates τ_m^{-1} and τ_p^{-1} respectively is given by $\bar{p} = \alpha_m \alpha_p \tau_m \tau_p$ (6). In the limit in which

extrinsic noise dominates over intrinsic fluctuations, the population variability is determined by diversity in these parameters among different cells. Assume for example that only the translation rate α_p varies between cells, due to variation in the number of ribosomes per cell. We distinguish two different scenarios in which protein numbers vary between experimental conditions: if the distribution of α_p does not change between experimental conditions and the change in protein numbers is due to changes in the other parameters, then for the i-th condition:

$$\left(\sigma_p^2\right)_i = \left(\alpha_m\tau_m\tau_p\right)_i^2\sigma_{\alpha_p}^2 = \left(\alpha_m\tau_m\tau_p\right)_i^2\bar{\alpha}_p{}^2\frac{\sigma_{\alpha_p}^2}{\bar{\alpha}_p{}^2} = \bar{p}_i{}^2\cdot\frac{\sigma_{\alpha_p}^2}{\bar{\alpha}_p{}^2}$$

Since in this case the ratio $\sigma_{\alpha p}^2/\bar{\alpha}_p{}^2$ is constant throughout the experimental conditions, a linear dependence between the standard deviation and the mean number of proteins ensues. This can represent for example a situation in which the transcription rate α_m varies between experimental conditions, with no effect on ribosome numbers in the cell. This is the situation studied in our stochastic computer simulations.

A different situation results if only α_p varies between experimental conditions, while other parameters remain constant. For instance, under stressful conditions the number of ribosomes changes. In this case we obtain:

$$\left(\sigma_p^2\right)_i = \left(\alpha_m\tau_m\tau_p\right)^2\left(\sigma_{\alpha_p}^2\right)_i = \left(\alpha_m\tau_m\tau_p\right)^2\left(\bar{\alpha}_p\right)_i^2\frac{\left(\sigma_{\alpha_p}^2\right)_i}{\left(\bar{\alpha}_p\right)_i^2} = \bar{p}_i{}^2\cdot\frac{\left(\sigma_{\alpha_p}^2\right)_i}{\left(\bar{\alpha}_p\right)_i^2}$$

A linear dependence of standard deviation on the mean is obtained only if α_p is drawn from a family of distribution such that the ratio $\left(\sigma_{\alpha p}^2\right)_i/\left(\bar{\alpha}_p\right)_i^2$ is constant. This constrains the type of possible distributions of α_p. For instance a Gamma distribution can obey this condition whereas a Poisson distribution cannot. Note that in our experiments both the distribution of α_p and τ_m vary with DTPA levels.

Attempts to measure intrinsic noise in SodB synthesis using strains bearing dual chromosomal SodB genes.

In an effort to test theoretical predictions concerning the possible non-monotonic behavior of intrinsic noise of proteins whose expression is down-regulated by a sRNA (15), we have prepared two strains bearing dual chromosomal copies of the sodB gene (SI Materials and Methods). Experiments to study intrinsic noise were carried out with both the above strains, following known procedures (15), for different concentrations of DTPA, and under the same conditions as the experiments reported in the Main Text. Measurements at the level of individual cells showed significant differences in the fluorescence intensities between SodB-CFP and SodB-YFP in both strains, under iron-rich conditions. While in the first strain the average fluorescence from SodB-YFP exceeded that of SodB-CFP by a factor of 5, in the second strain the

average fluorescence from SodB-CFP exceeded that of SodB-YFP by a factor of 2. The average fluorescence values of SodB-CFP in both strains were comparable to those measured in the FumA-YFP SodB-CFP strain used throughout our study. The differences in the expression level of SodB proteins in cells bearing two chromosomal copies of the sodB gene indicate that the duplicated gene copies are regulated by additional factors whose effects cannot be isolated in order to measure intrinsic noise directly in our model system. These results suggest that the chromosomal context of the inserted copies of the sodB genes is an important determinant in their expression, and that measurements of cell-to-cell fluctuations in dual gene fused reporter systems can be affected by additional unforeseen factors. A full account of these measurements will be published elsewhere.

Supplementary References

1. Levine, E., Zhang, Z., Kuhlman, T. and Hwa, T. (2007) Quantitative characteristics of gene regulation by small RNA. *PLoS Biol.*, **5**, e229.
2. So, L.H., Ghosh, A., Zong, C., Sepulveda, L.A., Segev, R. and Golding, I. (2011) General properties of transcriptional time series in Escherichia coli. *Nat. Genet.*, **43**, 554-560.
3. Ishihama, Y., Schmidt, T., Rappsilber, J., Mann, M., Hartl, F.U., Kerner, M.J. and Frishman, D. (2008) Protein abundance profiling of the Escherichia coli cytosol. *BMC Genomics*, **9**, 102.
4. Taniguchi, Y., Choi, P.J., Li, G.W., Chen, H., Babu, M., Hearn, J., Emili, A. and Xie, X.S. (2010) Quantifying E. coli proteome and transcriptome with single-molecule sensitivity in single cells. *Science*, **329**, 533-538.
5. Amir, A., Meshner, S., Beatus, T. and Stavans, J. (2010) Damped oscillations in the adaptive response of the iron homeostasis network of E. coli. *Mol. Microbiol.*, **76**, 428-436.
6. Mehta, P., Goyal, S. and Wingreen, N.S. (2008) A quantitative comparison of sRNA-based and protein-based gene regulation. *Mol. Syst. Biol.*, **4**, 221.
7. Guzman, L.M., Belin, D., Carson, M.J. and Beckwith, J. (1995) Tight regulation, modulation, and high-level expression by vectors containing the arabinose PBAD promoter. *J. Bacteriol.*, **177**, 4121-4130.
8. Svenningsen, S.L., Costantino, N., Court, D.L. and Adhya, S. (2005) On the role of Cro in lambda prophage induction. *Proc. Natl. Acad. Sci. USA*, **102**, 4465-4469.
9. Bubunenko, M., Baker, T. and Court, D.L. (2007) Essentiality of ribosomal and transcription antitermination proteins analyzed by systematic gene replacement in Escherichia coli. *J. Bacteriol.*, **189**, 2844-2853.
10. Sharan, S.K., Thomason, L.C., Kuznetsov, S.G. and Court, D.L. (2009) Recombineering: a homologous recombination-based method of genetic engineering. *Nat Protoc*, **4**, 206-223.
11. Baba, T., Ara, T., Hasegawa, M., Takai, Y., Okumura, Y., Baba, M., Datsenko, K.A., Tomita, Wanner, B.L. and Mori, H. (2006) Construction of Escherichia coli K-12 in-frame, single-gene knockout mutants: the Keio collection. *Mol. Syst. Biol.*, **2**, 0008.
12. Rosenfeld, N., Young, J.W., Alon, U., Swain, P.S. and Elowitz, M.B. (2005) Gene regulation at the single-cell level. *Science*, **307**, 1962-1965.

13. Gillespie, D.T. (1977) Exact stochastic simulation of coupled chemical-reactions *J. Phys. Chem.*, **81**, 2340-2361.
14. Bremer, H. and Dennis, P.P. (1996) In Neidhardt, F. C., Curtiss, I. R., Ingraham, J. L., Lin, E. C. C., Low, K. B., Magasanik, B., Reznikoff, W. S., Riley, M., Schaechter, M. and Umbarger, H. E. (eds.), *Escherichia coli and Salmonella: cellular and molecular biology*. 2nd ed. ASM Press, Washington, D.C., pp. 1553–1569.
15. Elowitz, M.B., Levine, A.J., Siggia, E.D. and Swain, P.S. (2002) Stochastic gene expression in a single cell. *Science*, **297**, 1183-1186.